Article

Direct Route to Tungsten Oxide Nanorod Bundles: Microstructures and Electro-Optical Properties

Cherng-Yuh Su, and Hsuan-Ching Lin

J. Phys. Chem. C, **2009**, 113 (10), 4042-4046• DOI: 10.1021/jp809458j • Publication Date (Web): 13 February 2009

Direct Route to Tungsten Oxide Nanorod Bundles: Microstructures and Electro-Optical Properties

Cherng-Yuh Su* and Hsuan-Ching Lin

Institute of Manufacturing Technology, National Taipei University of Technology, Taipei, Taiwan

Received: October 25, 2008; Revised Manuscript Received: January 11, 2009

In the present research, tungsten oxide nanorod bundles were synthesized by a unique plasma arc gas condensation method that was both noncatalytic and template-free. $W_{18}O_{49}$ nanorod bundles were prepared by directly evaporating tungsten bulk in an oxygen-deficient environment. The as-prepared tungsten oxide nanorod bundles were characterized by FESEM, HRTEM, XRD, UV−visible spectroscopy, and PL measurements. The field-emission property was also evaluated. FESEM images showed bundlelike morphology; XRD and HRTEM results confirmed that the nanorod bundles were in a single-crystalline monoclinic $W_{18}O_{49}$ phase, with the growth direction along [010]. Also, oxygen deficiencies within the nanostructures induced the red-shift phenomenon and blue emission observed in the UV−visible and photoluminescence spectra. The field-emission measurement showed that the tungsten oxide nanorod bundles exhibited low turn-on and threshold voltages, which were about 3.5 and 4.6 V/μm, respectively. These results indicate that the tungsten oxide nanorod bundles are a promising candidate for field-emitter applications.

1. Introduction

Recently, 1D materials have provided a means to investigate the effects of low dimensionality on their physical and chemical properties.[1,2] Because of their unique architectures, 1D materials also offer an opportunity to fabricate certain nanodevices.[3,4] Among the metal oxide materials, tungsten oxide (WO_x, $2 < x < 3$), an important semiconductor material with a wide band gap ranging from 2.5 to 3.5 eV, is of great interest because of its practical applications in smart windows,[5] photocatalysts,[6] and gas/temperature sensors.[7,8] Therefore, much effort has been expended to synthesize 1D tungsten oxide materials with various morphologies and phases using either physical or chemical routes.[9−20]

Among the various phases in the WO_3 system, the nonstoichiometric phase (i.e., the WO_{3-x} form) has attracted much interest because of its unique structural plane and the oxygen defects within its nanostructures.[21,22] For example, Li et al. synthesized $W_{18}O_{49}$ nanotubes and nanowires through the irradiation heating of a W foil on a Ta wafer as a substrate. The field-emission property was also investigated.[9] Large-scale $W_{18}O_{49}$ nanoneedles were obtained by a chemical vapor deposition (CVD) process using simple tungsten metals reacting with water at 800−1000 °C. Furthermore, spiky-ball and bundlelike products could be prepared by altering the W source and experimental conditions.[10] Quasi-aligned $W_{18}O_{49}$ nanotip arrays were prepared by a two-step evaporation deposition process, and they exhibited excellent field-emission properties with low turn-on and threshold voltages as a result of their higher aspect ratio.[11] By simply heating an array of tungsten filaments, $W_{18}O_{49}$ nanowires/nanobundles and WO_3 3D nanowire networks have been synthesized. The effects of substrate temperatures on the nanostructures were also revealed.[12] Shi et al. also promoted a low-temperature method (600 °C) of preparing $W_{18}O_{49}$ nanowires by reacting tungsten powders and water vapor, and their temperature-dependent electrical transport properties were also investigated.[13] As these studies make clear, catalysts or substrates are required during the process. To simplify the synthesis process and minimize contaminants, a feasible, effective method is required.

Our previous study developed a noncatalytic, template-free modified plasma arc gas condensation system to prepare WO_3 and WO_{3-x} nanomaterials with a yield rate of a few hundred grams per hour.[23] We also transferred from 0D tungsten oxide nanoparticles to nonstoichiometric tungsten oxide nanorods by adding hydrogen (H_2) as a reductive plasma gas.[24]

In the present research, we prepared unique $W_{18}O_{49}$ nanorod bundles using a unique process by directly evaporating tungsten bulk in an oxygen-deficient environment. Investigations of the microstructures and electro-optical properties of the as-prepared tungsten oxide nanorod bundles are discussed. In addition, a possible growth mechanism for the bundlelike structure is also proposed.

2. Experimental Methods

The tungsten oxide nanorods bundles were directly prepared by a high-temperature physical route without substrates and catalysts, which was described in earlier work.[23,24] Bulk tungsten (99.95% purity, Ample Goal International, Co. Ltd, Japan) was placed in a copper crucible and evaporated with a high-energy plasma arc. An inlet gas nozzle placed close to the plasma was used to introduce argon and oxygen in a ratio of 10/1. Dynamic gas pressure equilibrium was carefully maintained at a pressure of 760 Torr during experimental processing. After the experiment was carried out, the final dark-blue products were collected. The processing parameters are summarized in Table 1.

The surface morphology and the microstructure of the as-prepared tungsten oxide nanomaterials were characterized by field-emission scanning electron microscopy (FESEM, JSM-6500F, JEOL, Japan) and analytical transmission electron microscopy with energy-dispersive spectrometry (AEM/EDS, JEM-2010, JEOL, Japan). Additionally, an X-ray diffractometer (XRD, X'Pert PRO MPD, PANalytical, Holland) with mono-

* Corresponding author. Tel: +886-2-27716117 ext. 2044. Fax: +886-2-27317191. E-mail: cysu@ntut.edu.tw.

10.1021/jp809458j CCC: $40.75
Published on Web 02/13/2009

TABLE 1: Processing Parameters

plasma current	90 A
plasma voltage	34 V
shielding gas (Ar)	10 SCFH
plasma gas (He)	3 SCFH
blowing gas (Ar/O_2)	10/1
chamber pressure	760 Torr
gas purity (Ar or O_2)	99.99%
arc length	<1 cm
setback	0.236 cm

chromatic Cu Kα radiation was used to determine the phase of the tungsten oxide nanomaterials.

To evaluate the optical properties of the as-prepared tungsten oxide nanomaterials, a UV−visible absorption spectrum (Helios Alpha, Thermo Spectronic, U.K.) and a photoluminescence (PL) measurement (Hitachi F-4500, fluorescence spectrometer at an excitation of 325 nm) were used at room temperature. The sample was first adhered to a high-conductivity copper disk with an oxygen-free surface using silver paint. The gap between the anode and the cathode was 250 μm. The field-emission properties of the as-prepared nanomaterials were examined in a vacuum chamber at a pressure of less than 2×10^{-6} Torr.

3. Results and Discussion

It should be noted that the final products of the experiment were dark blue, indicating that the tungsten oxide was in a nonstoichiometric phase. As shown in Figure 1a, an FESEM image of the as-prepared tungsten oxide nanomaterials shows clearly a bundlelike structure with a diameter of about 1 to 2 μm. A high-magnification FESEM image shown in Figure 1b reveals the detailed morphology of the bundlelike structures. Each bundle is composed of many nanorods that are 20 to 30 nm in diameter, aligned parallel and agglomerated to form bundles.

Although some tungsten oxide nanobundles have been synthesized previously, the unique bundlelike morphology of our as-prepared products is quite interesting and different from that of previous studies because of our use of different synthesis processes and growth mechanisms.[10,16] The unique nanostructure may be attributed to the temperature gradient between the heating source and the target. In addition, the competing growth process between the nanorods leads to the unique structures as well.[12]

The phase identification of the as-prepared tungsten oxide nanorod bundles was performed by the XRD technique. Figure 2a shows the typical XRD pattern for as-prepared tungsten oxide nanorod bundles. All peaks were indexed well to the monoclinic-phase $W_{18}O_{49}$ crystal simulation profile in Figure 2b with lattice constants; $\beta = 115.2°$, $a = 1.8334$nm, $b = 0.3876$ nm, and $c = 1.4004$ nm (JCPDS card no. 71-2450). In addition, the major peak in the XRD pattern was a (010) plane. This corresponded to the close-packed plane of the $W_{18}O_{49}$ crystals, suggesting that the dominant growth direction of the as-prepared tungsten oxide nanorod bundles was along the close-packed plane.

The microstructure of the $W_{18}O_{49}$ nanorod bundles was characterized using transmission electron microscopy (TEM). Figure 3a is a typical low-magnification TEM image of nanorod bundles. It is obvious that nanorods coalesce into a bundlelike structure. The arrow indicates the boundary between two nanorods, which corresponds to SEM images. A high-resolution TEM (HRTEM) image of a $W_{18}O_{49}$ nanorod, shown in Figure 3b, reveals that lattice spacings of 0.378 and 0.373 nm can be indexed. The spacing correspond to the (010) and (103) planes,

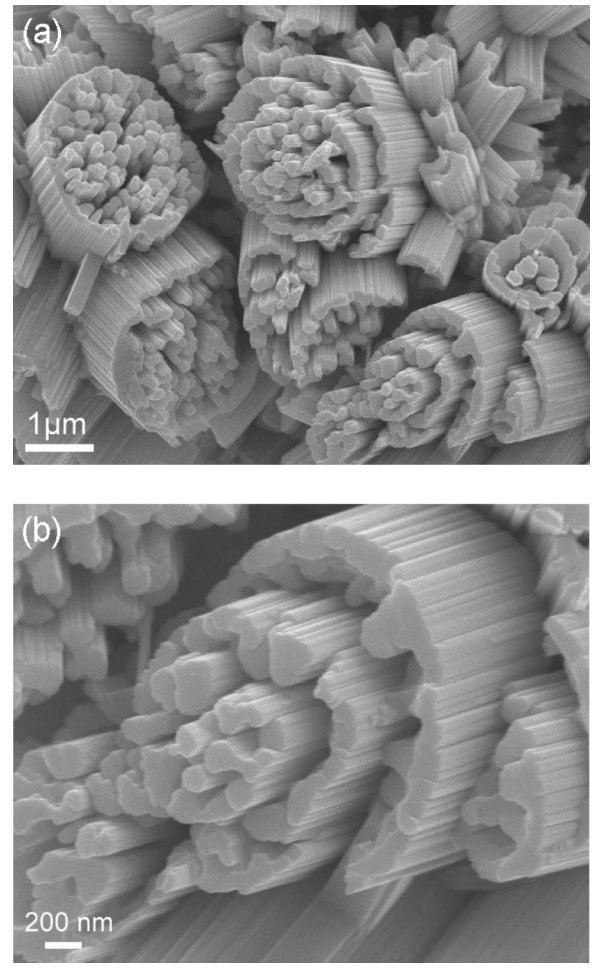

Figure 1. Typical FESEM images of tungsten oxide nanorods bundles at (a) low magnification and (b) high magnification.

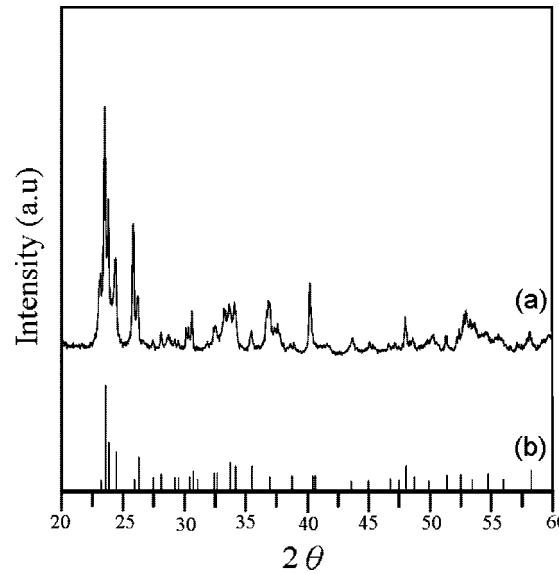

Figure 2. XRD patterns of (a) the as-prepared tungsten oxide nanorod bundles and (b) JCPDS card no. 71-2450.

respectively. Recall the XRD pattern shown in Figure 2, where the dominant growth orientation of the $W_{18}O_{49}$ nanorod is in the [010] direction. The selected-area electron diffraction (SAED) pattern seen in Figure 3b is presented in Figure 3c, which shows that the nanorod had a single-crystalline structure. For the chemical composition analysis, the energy-dispersive

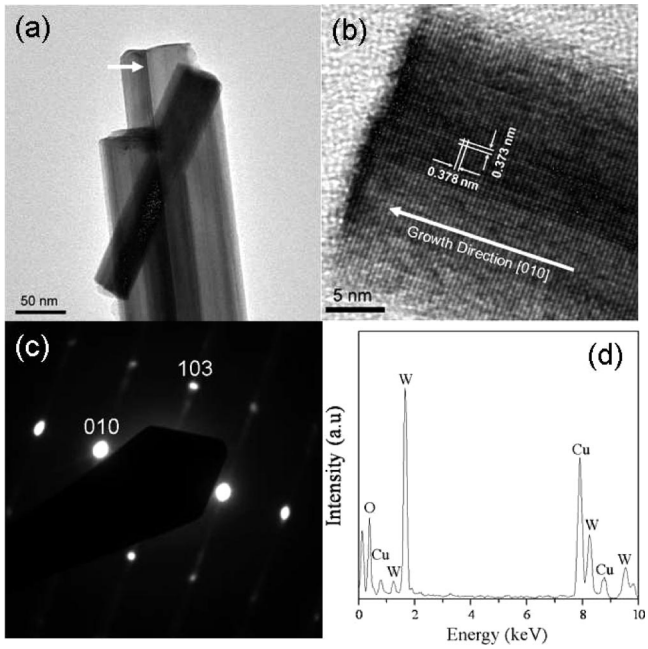

Figure 3. (a) Low-magnification TEM image of nanorod bundles, with the arrow indicating the boundary between two nanorods. (b) High-resolution TEM (HRTEM) image of a single $W_{18}O_{49}$ nanorod with an approximate diameter of 25 nm. (c, d) Selected-area electron diffraction (SAED) pattern and the energy dispersive X-ray spectroscopy (EDS) analysis of a $W_{18}O_{49}$ nanorod, respectively.

spectrometer (EDS) spectrum taken from a single nanorod (Figure 3d) suggests that the nanorods mainly consist of tungsten and oxygen with an atomic W/O ratio of 1/2.735, which is close to that of $W_{18}O_{49}$ and consistent the XRD and TEM results.

On the basis of the FESEM and HRTEM characterization results, we suggested that the growth model for the nanorod bundles may be explained by the vapor-solid process.[25] First, the tungsten bulk is evaporated by the high-energy plasma arc and oxidized rapidly. The evaporated tungsten oxide molecules attach on the surface of the collector and serve as the "leading nuclei."[26] Nonstoichiometric tungsten oxide nanoparticles (i.e., WO_{3-x}) are formed as a result of the limited number of oxygen molecules in the chamber. Evaporated tungsten oxide molecules are continuously provided by the system and quickly become superfluous. Instead of growing into equiaxis particles, the temperature gradient between the heating source and collector induces WO_{3-x} nanoparticles to stack along the oxygen-deficient direction and grow into nanorods. Finally, the nanorods aggregate into bundlelike structures to reduce the interfacial energy between the nanorods, as revealed in Figure 3a.

The optical absorption spectrum of the $W_{18}O_{49}$ nanorod bundles was measured at room temperature. Figure 4 shows the UV−visible spectrum of the $W_{18}O_{49}$ nanorod bundles. It is notable that the absorption wavelength is approximately ∼420 nm and the band gap value of the $W_{18}O_{49}$ nanorod bundles is ∼2.95 eV, as estimated by the $(\alpha E)^2 - E$ curve (Figure 4 inset). Compared with the absorption wavelength value (∼360 nm) of WO_3 nanoparitcles,[27] the $W_{18}O_{49}$ nanorod bundles exhibited the red-shift phenomenon at an optical absorption wavelength. It has been reported that the size distribution and crystallinity of the tungsten oxide nanomaterials will influence the band gap values.[28,29] Oxygen deficiencies also play an important role. The effects of oxygen concentration on the optical properties of annealed WO_3 nanorods/films have been investigated, and it appears that the higher annealing temperature makes WO_3 nanorods/films more dense and causes them to form more

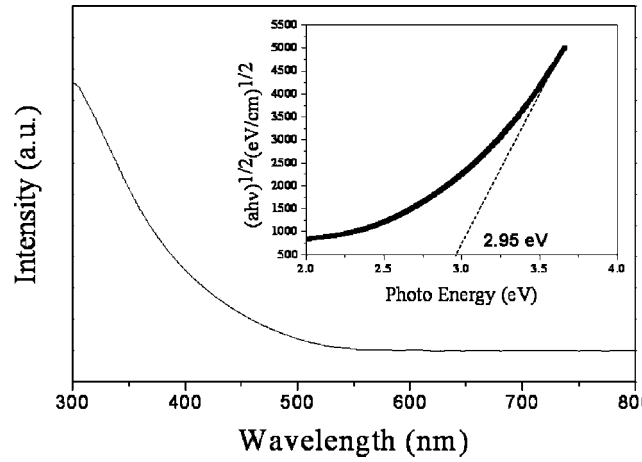

Figure 4. UV−visible spectrum of the as-prepared $W_{18}O_{49}$ nanorod bundles. The inset is the corresponding $(\alpha E)^2 - E$ curve.

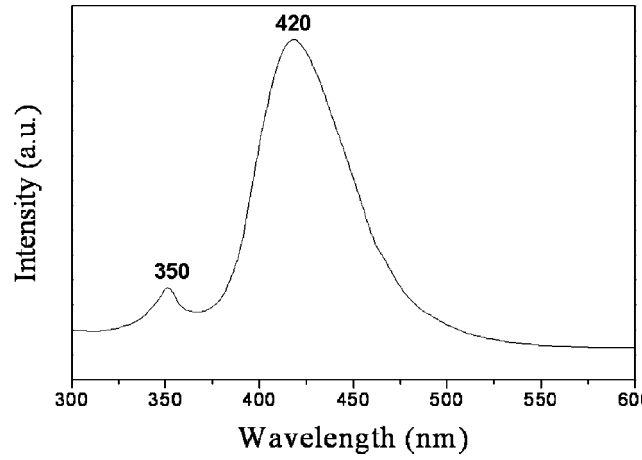

Figure 5. Photoluminescence (PL) spectrum of the as-prepared $W_{18}O_{49}$ nanorod bundles.

oxygen ion deficiencies. This decreases their band gap value from 3.30 to 2.0 eV.[30] Therefore, the oxygen deficiencies within the nanostructures were responsible for the decrease in the band gap value of the $W_{18}O_{49}$ nanorod bundles in the present research.

As far as we know, few literature reports on the PL properties of tungsten oxide nanomaterials exist. Figure 5 shows the room-temperature PL spectrum of the as-prepared $W_{18}O_{49}$ nanorod bundles. When excited at 325 nm, two PL characteristic peaks can be induced: one is at 350 nm (3.54 eV), and the other is at 420 nm (2.95 eV). Lee et al. also observed a similar PL peak at a wavelength of 350 nm and inferred that this characteristic peak may be attributed to the intrinsic band-to-band transition emission induced by quantum confinement effects within the nanostructures.[31] However, another strong-intensity blue emission at 420 nm was observed, and may have originated from defects such as oxygen deficiencies or other impurities.[32] However, it is interesting that the blue emission was shorter than that reported previously. It ranged from 423 to 437 nm,[31−33] indicating that the nanoscale size effect might have taken place. In the PL spectrum, the intensity of the blue-emission peak was much higher than that of a band-to-band emission peak, which is due to more oxygen vacancies existing in the nanorod bundle structures, as reported by Li's group.[33]

Figure 6 shows a current density (J) versus applied voltage (E) plot for the as-prepared $W_{18}O_{49}$ nanorod bundles, when measured using an anode−cathode gap of 250 μm in a vacuum pressure of 2×10^{-6} Torr. The measurement went through many

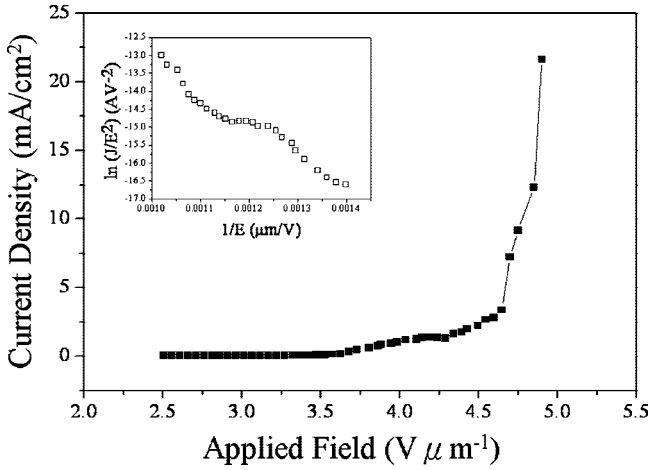

Figure 6. Field-emission current density vs applied field ($J-E$) of the as-prepared $W_{18}O_{49}$ nanorod bundles. The inset is the corresponding F−N plot.

times, and the emission eventually seemed to reach a stable stage. According to the definitions of turn-on and threshold voltages at current densities of 10 μA/cm^2 and 10 mA/cm^2, the low turn-on and threshold voltages were about 3.5 and 4.6 V/μm, respectively. The variations of the turn-on and threshold voltages depend on the morphologies, chemical compositions, and phases of the measured materials. Meanwhile, the turn-on voltage of the $W_{18}O_{49}$ nanorod bundles was lower than those of the Cu_2S nanowires (~6 V/μm),[34] $W_{18}O_{49}$ nanorods (~9.5 V/μm),[20] and WO_3 nanowire networks (~13.85 V/μm).[35] However, their turn-on voltage was close to that of CuO nanowire films (3.5−4.5 V/μm),[36] ZnS nanobelts (~3.47 V/μm),[37] and MoO_3 nanowires (~3.5 V/μm).[38] Interestingly, the maximum current density of 21.7 mA/cm^2 (under an applied field of 4.89 Vμm^{-1}) was superior to that of other tungsten oxide 1D nanomaterials.[9,11,14,20,35] This unique phenomenon can be explained by the collective contribution of the individual nanorods in the bundles. In addition, a fluctuation curve from the voltage field applied at 3.5 eV can be observed in the $J-E$ plot. The curve may be attributed to the stress within the nanostructures at high applied voltage.[15]

A Fowler−Nordheim (F−N) plot was used to analyze and reveal the field-emission behavior.[39] As shown in the inset in Figure 6, the corresponding F−N plot was depicted in the following F−N equation

$$J = (\beta^2 E^2/\Phi)\exp(-B\Phi^{3/2}/\beta E)$$

where J is the current density, E is the applied field, Φ is the work function of tungsten oxide (5.7 eV),[40] β is the field enhancement factor, and B is a constant corresponding to 6.83 $\times$ 10^3 [V(eV$^{-3/2}$)(μm^{-1})]. The F−N plot exhibits nonlinearity, indicating that the different β values exist in high- and low-field regions. Recall the FESEM images shown in Figure 1. The $W_{18}O_{49}$ nanorod bundles are composed of many nanorods with different lengths and diameters, so field enhancement factors also vary to create different turn-on voltages.[34] In addition, the desorption of absorbates originates from water/gas molecules on the surface of the tungsten oxide nanorod bundles, possibly leading to nonlinearity in the F−N plot.[35] From the slope ($-B\Phi^{3/2}/\beta$) of the F−N plot, the corresponding field enhancement factors in high- and low-field regions were estimated to be 2269 and 2131, which are high enough for various field-emission applications. The barrier-tunneling process is responsible for the field-emission behavior as well.[39] The nanorod bundles in the present research, if mass- produced, could have economical potential in flat displays in the near future.

4. Conclusions

In summary, $W_{18}O_{49}$ nanorod bundles were prepared successfully by a modified plasma arc gas condensation technique without any catalysts and substrates. XRD and HRTEM results showed that the nanorod bundles were in a single-crystalline monoclinic $W_{18}O_{49}$ phase and that the growth direction was along the [010] plane. The oxygen defects within the nanostructures could explain the red-shift phenomenon and blue-emission optical properties. Field-emission measurements showed that the $W_{18}O_{49}$ nanorod bundles exhibit low turn-on and threshold voltages of 3.5 and 4.6 V/μm, respectively. These results indicate that the $W_{18}O_{49}$ nanorod bundles have great potential in field-emission applications.

Acknowledgment. This work was supported by the National Science Council of Taiwan under contract nos. NSC94-2216-E-027-008 and NSC95-2216-E-027-009. We thank Professor Yuan-Hsiang Yu at Lan Yang Institute of Technology for support and discussions of the field-emission measurement. XRD technical support from the College of Engineering at National Taipei University of Technology is also acknowledged.

References and Notes

(1) Ruecks, T.; Kim, K.; Joselevich, E.; Tseng, G. Y.; Cheung, C.; Lieber, C. M. *Science* **2000**, *289*, 84.
(2) Huang, M. H.; Mao, S.; Feick, H.; Yan, H.; Wu, Y.; Kind, H.; Weber, E.; Russo, R.; Yang, P. *Science* **2001**, *292*, 1897.
(3) Wu, J.; Eastman, M.; Gutu, T.; Wyse, M.; Jiao, J.; Kim, S. M.; Mann, M.; Zhang, Y.; Teo, K. B. K. *Appl. Phys. Lett.* **2007**, *91*, 173122.
(4) Liao, L.; Zheng, Z.; Yan, B.; Zhang, J. X.; Gong, H.; Li, J. C.; Liu, C.; Shen, Z. X.; Yu, T. *J. Phys. Chem C* **2008**, *112*, 10784.
(5) Niklasson, G. A.; Granqvist, C. G. *J. Mater. Chem.* **2007**, *17*, 127.
(6) Sayama, K.; Mukasa, K.; Abe, R.; Abe, Y.; Arakawa, H. *Chem. Commun.* **2001**, *23*, 2416.
(7) Reyes, L. F.; Hoel, A.; Saukko, S.; Heszler, P.; Lantto, V.; Granqvist, C. G. *Sens. Actuators, B* **2006**, *117*, 128.
(8) Ho, J. *Solid-State Electron.* **2003**, *47*, 827.
(9) Li, Y.; Bando, Y.; Golberg, D. *Adv. Mater.* **2003**, *15*, 1294.
(10) Jin, Y. Z.; Zhu, Y. Q.; Whitby, R. L. D.; Yao, N.; Ma, R.; Wats, P. C. P.; Kroto, H. W.; Walton, D. R. M. *J. Phys. Chem. B* **2004**, *108*, 15572.
(11) Zhou, J.; Gong, L.; Deng, S. Z.; Chen, J.; She, J. C.; Xu, N. S.; Yang, R.; Wang, Z. L. *Appl. Phys. Lett.* **2005**, *87*, 223108.
(12) Chi, L.; Xu, N.; Deng, S.; Chen, J.; She, J. *Nanotechnology* **2006**, *17*, 5590.
(13) Shi, S.; Xue, X.; Feng, P.; Liu, Y.; Zhao, H.; Wang, T. *J. Cryst. Growth* **2008**, *310*, 143.
(14) Liu, J.; Zhang, Z.; Zhao, Y.; Su, Z.; Liu, S.; Wang, E. *Small* **2005**, *3*, 310.
(15) Cheong, F. C.; Varghese, B.; Zhu, Y.; Tan, E. P. S.; Dai, L.; Tan, V. B. C.; Lim, C. T.; Sow, C. H. *J. Phys. Chem. C* **2007**, *111*, 17193.
(16) Sun, S.; Zhao, Y.; Xia, Y.; Zou, Z.; Min, G.; Zhu, Y. *Nanotechnology* **2008**, *19*, 305709.
(17) Wu, Y.; Xi, Z.; Zhang, G.; Yu, J.; Guo, D. *J. Cryst. Growth* **2006**, *292*, 143.
(18) Yoo, S. J.; Lim, Y. J.; Sung, Y. E.; Jung, Y. H.; Choi, H. G.; Kim, D. K. *Appl. Phys. Lett.* **2007**, *90*, 173126.
(19) Wang, X. P.; Yang, B. Q.; Zhang, H. X.; Feng, P. X. *Nanoscale Res. Lett.* **2007**, *2*, 405.
(20) Jeon, S.; Yong, K. *Nanotechnology* **2007**, *18*, 245602.
(21) Frey, G. L.; Rothschild, A.; Sloan, J.; Rosentsveig, R.; Popovitz-Birom, R.; Tenne, R. *J. Solid State Chem.* **2001**, *162*, 300.
(22) Lou, X. W.; Zeng, H. C. *Inorg. Chem.* **2003**, *42*, 6169.
(23) Su, C. Y.; Lin, C. K.; Cheng, C. W. *Mater. Trans.* **2005**, *46*, 1016.
(24) Su, C. Y.; Lin, C. K.; Yang, T. K.; Lin, H. C.; Pan, C. T. *Int. J. Refract. Met. Hard Met.* **2008**, *26*, 423.
(25) Ma, Y. R.; Lin, C. M.; Yeh, C. L.; Huang, R. T. *J. Vac. Sci. Technol., B* **2005**, *23*, 2141.

(26) Pfeifer, J.; Badaljan, E.; TekulabBuxbaum, P.; Kovacs, T.; Geszti, O.; Toth, A. L.; Lunk, H. J. *J. Cryst. Growth* **1996**, *169*, 727.
(27) He, T.; Ma, Y.; Cao, Y.; Hu, X.; Liu, H.; Zhang, G.; Yang, W.; Yao, J. *J. Phys. Chem. B* **2002**, *106*, 12670.
(28) Li, X.; Zhang, G.; Cheng, F.; Guo, B.; Chen, J. *J. Electrochem. Soc.* **2006**, *153*, H133.
(29) Subrahmanyam, A.; Karuppasamy, A. *Sol. Energy Mater. Sol. Cells* **2007**, *91*, 266.
(30) Smith, W.; Zhang, Z. Y.; Zhao, Y. P. *J. Vac. Sci Technol., B* **2007**, *25*, 1875.
(31) Feng, M.; Pan, A. L.; Zhang, H. R.; Li, Z. A.; Liu, F.; Liu, H. W.; Shi, D. X.; Zou, B. S.; Gao, H. J. *Appl. Phys. Lett.* **2005**, *86*, 141901.
(32) Lee, K.; Seo, W. S.; Park, J. T. J. *J. Am. Chem. Soc.* **2003**, *125*, 3408.
(33) Li, Y. H.; Zhao, Y. M.; Ma, R. Z.; Zhu, Y. Q.; Fisher, N.; Jin, Y. Z.; Zhang, X. P. *J. Phys. Chem. B* **2006**, *110*, 18191.
(34) Chen, J.; Deng, S. Z.; Xu, N. S.; Wang, S. H.; Wen, X. G.; Yang, S. H.; Yang, C. L.; Wang, J. N.; Ge, W. K. *Appl. Phys. Lett.* **2002**, *80*, 3620.
(35) Zhou, J.; Dong, Y.; Deng, S. Z.; Gong, L.; Xu, N. S.; Wang, Z. L *Adv. Mater.* **2005**, *17*, 2107.
(36) Zhu, Y. W.; Yu, T.; Cheong, F. C.; Xu, X. J.; Lim, C. T.; Tan, V. B.; Thong, J. T. L.; Sow, C. H. *Nanotechnology* **2005**, *16*, 88.
(37) Fang, X.; Gautam, U. K.; Bando, Y.; Dierre, B.; Sekiguchi, T.; Golberg, D. *J. Phys. Chem. C* **2008**, *112*, 4635.
(38) Zhou, J.; Xu, N. S.; Deng, S. Z.; Chen, J.; She, J. C.; Wang, Z. L. *Adv. Mater.* **2003**, *15*, 1835.
(39) Fowler, R. H.; Nordheim, L. W *Proc. R. Soc. London* **1928**, *119*, 173.
(40) Gillet, M.; Delamare, R.; Gillet, E. *Eur. Phys. J. D* **2005**, *34*, 291.

JP809458J